Journal of Geochemical Exploration 160 (2016) 31–43

Contents lists available at ScienceDirect

Journal of Geochemical Exploration

journal homepage: www.elsevier.com/locate/jgeoexp

Computational simulation of coupled geodynamics for forming the Makeng deposit in Fujian Province, China: Constraints of mechanics, thermotics and hydrology

Xiaoqiao Gao, Da Zhang *, Vatuva Absai, Haibin Feng, Jinjun Yi

School of Earth Sciences and Resources, China University of Geosciences, Beijing 100083, China

A R T I C L E   I N F O

Article history:
Received 18 May 2015
Revised 3 October 2015
Accepted 15 October 2015
Available online 17 October 2015

Keywords:
Numerical simulation
Coupled geodynamics
Makeng deposit
Dilation space
Ore localization

A B S T R A C T

The Makeng Fe (–Mo) deposit is the largest iron deposit in the Southwestern Fujian metallogenic belt of southeast China. This deposit's genesis has been disputed since the 1950s, with the primary view being that of the skarn type. Detailed geological investigations of the deposit were conducted to elucidate the ore-forming processes at work, as well as its localization. The investigations were based on computational geodynamic models that were, in turn, constructed by simulating the syn-extensional cooling of the ore-related intrusion. We have developed a FISH program to transform the MIDAS/GTS geometric solid model into the FLAC3D geodynamic discrete model. The occurrence of the granite xenoliths in ores and the sharp boundary of the ore body suggest that the ore body was formed at the tensile fracture spaces of the host rocks. The results of the numerical simulation show that most ore bodies are located in the weak zones of the limestone strata with dilation zones that are well-developed. Thus, the fluids from different sources can be easily focused due to the coupled mechano–thermo-hydrological (MTH) processes. The ore forming processes are closely related to the mechanical properties of sedimentary strata, especially regarding its competence and the contact relationship with different rock units. The computational model shows the same depth found through deep geological drilling, which also identified significant ore bodies. The simulation model will facilitate the selection of targets for further exploration of concealed deposits.

1. Introduction

The demand for iron is increasing everyday due to massive construction projects in China and around the world. Readily discoverable ore deposits are increasingly becoming depleted. As a result, there is a need to study the existing deposits in detail to establish models that can be used to facilitate the selection of targets for exploring concealed ore deposits. The formation of hydrothermal deposits and their occurrence are a result of complex metallogenic and coupled geodynamics processes (Hobbs et al., 2000, 2004; Hornby et al., 2006a,b, 2008; Poulet et al., 2013; Price and Stoker, 2002; Zhao et al., 2008a, 2009). Generally, hydrothermal mineralization arises from a complex interplay of deformation, fluid flow, conductive and advective heat transfer, solute transport and chemical reactions (Liu et al., 2011; Zhao et al., 2008b, 2009). Conventional exploration methods are increasingly becoming ineffective at maximizing the probability of ore discovery while minimizing the discovery cost. The advancement of computer technology and computational algorithms has enabled computational simulation to serve as an indispensable method for solving this problem. Simulating the thermo–mechano-hydrological processes of ore formation with computational algorithms is therefore necessary to depict the ore genesis and its forming mechanism, which is useful in predicting ore locations (Eldursi et al., 2008; Sheldon, 2009; Liu et al., 2011, 2012, 2014). Based on this idea, Zhao and his coworkers have conducted extensive original and pioneering research work (Zhao et al., 2008b, 2009; Zhao, 2009, 2014) to establish the emerging computational geoscience discipline over the last two decades (Awadh et al., 2013; Charifo et al., 2013; Schmidt Mumm et al., 2010). The developed computational geoscience methods (Peng et al., 2008, 2011; Reid et al., 2012a,b; Zhao et al., 1998, 2009; Zhao, 2015) have been successfully applied to the numerical simulation of several large ore deposits by many previous researchers (Garven and Freeze, 1984; Gow et al., 2002; Ju et al., 2011; Lin et al., 2002, 2006; Liu et al., 2005, 2010a, 2011; Ord et al., 2002, 2008b, 2010, 2012; Schaubs and Zhao, 2002; Sorjonen-Ward et al., 2002; Zhang et al., 2003, 2008; Zhao et al., 2014).

The Southwestern Fujian metallogenic belt (SFMB) is one of China's most important iron polymetallic metallogenic belts, in which many iron deposits have been discovered, including the Makeng, Yangshan, Pantian, Luoyang and Zhongjia iron deposits. These deposits are commonly referred to as the “Makeng type” iron

* Corresponding author at: China University of Geosciences (Beijing), Beijing 100083, China.
E-mail address: zhangda@cugb.edu.cn (D. Zhang).

http://dx.doi.org/10.1016/j.gexplo.2015.10.010
0375-6742/

deposits due to their close association with the super-large Makeng deposit. Geochemical processes play an important role in ore body formation and mineralization (Hobbs et al., 2007, 2008; Zhao et al., 2010, 2012; Zhao, 2014); thus, most previous studies (Chen et al., 1985; Chen, 2002, 2010; Ge et al., 1981; Jiang, 2009; Lin, 2008; Wang et al., 1981, 2015; Zhang, 2012; Zhang et al., 2012a; Zhang and Zuo, 2014) have mainly employed geochemical methods in resolving the genesis of the Makeng deposit. There are several models which describe the genesis of the Makeng iron deposit (Di et al., 2012), including (1) marine sedimentary (Chen, 2002; Lin, 2008); (2) marine volcanic sedimentary and hydrothermal re-working (Chen et al., 1985; Ge et al., 1981; Jiang, 2009; Wang et al., 1981); and (3) skarn-type iron deposit (Chen, 2010; Zhang, 2012; Zhang et al., 2012a; Zuo et al., 2012a). The source of iron metals and mineralizing fluids are the main source of the arguments (Zhang and Zuo, 2014). Recent studies (Chen, 2010; Zhang, 2012; Zuo et al., 2012a,b; Zhang et al., 2015) indicated that the Makeng iron deposit is a stratum-bound, skarn type deposit. Zhang and Zuo (2014) stated that the Yanshanian granitic intrusions provided heat, fluids and ore materials. Based on fluid inclusion studies, Zhang et al. (2013) recognized three groups of mineralization temperatures: 600–450 °C, 540–260 °C and 400–160 °C, indicating that ore formation is also dependent on temperature (Lin et al., 2003; Zhao et al., 2015a,b). Based on H, O, C and S isotope geochemical studies, Zhang et al. (2013) established that the main ore forming fluids are derived from magmatic waters, which indicates a generic relationship between Yanshanian Juzhou–Dayang granite suites and mineralization.

Quantitative analysis of the structural deformation in different areas, fluid flow mechanisms and structural control of the mineralization are seldom investigated on Makeng type deposits. Based on the geological evidence, the critical controls on the localization of ore-forming fluids at the deposit scale are temperature, dilation, fluid flow and fluid focusing; these processes are controlled by the temperature of the intrusion, the rheological and permeability contrasts, the structures of the system, and the stress regime at the time of mineralization. Thus, in this paper, we model and discuss the coupled geodynamics of the Makeng deposit as a function of mechanics, thermotics and hydrology. The simulation model provides a reference and basis for further exploration of the concealed deposit in this ore district. This paper also provides a tested method of modeling complex distinct geological bodies to resolve their metallogeny and thus further encourages the application of the emerging computational geoscience method to the broader geological research (Xing et al., 2008; Alt-Epping and Zhao, 2010; Lei et al., 2013).

2. Geological setting

The famous Makeng deposit is located in Longyan, Fujian Province. This deposit is the largest iron deposit in southeastern China, hosting ~450 Mt of ore body reserve. The deposit is formed in the early Hercynian Yong'an–Meixian depression on a Caledonian basement (Ge et al., 1981) and is part of the Southwestern Fujian metallogenic belt (SFMB). The major sedimentary rock in this belt consists of the Late Paleozoic formation. The middle–upper Carboniferous and lower Permian formation contain marine carbonate rocks and clastic rocks,

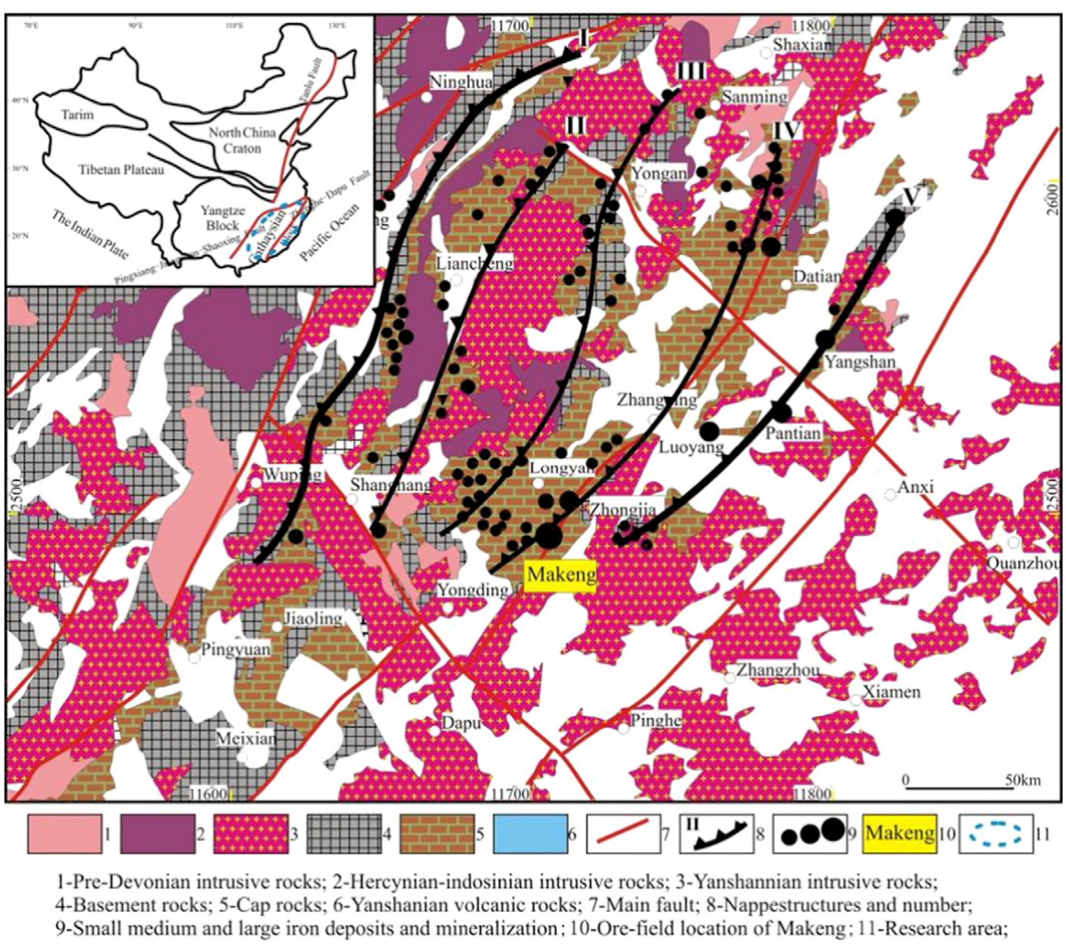

Fig. 1. Geological sketch map of Southwestern Fujian Province.
After Zhang et al. (2011).

which are the primary ore-hosting rock units. Voluminous Indosinian and Yanshanian granites intruded into the SFMB. Moreover, a few Hercynian diabases are emplaced in the region (Zhang et al., 2012a). Several Mesozoic belts of nappe structures (Fig. 1) extend from the west to the east of the SFMB. The nappes are divided into three stages that are characterized by different episodes of deformation: D1, late-Indosinian, late Triassic–early Jurassic (T_3–J_1); D2, early-Yashannian, middle Jurassic–early Cretaceous (J_2–K_1); and D3, late-Yashannian, late Cretaceous (the end of K_2). The D2 (175–140 Ma) is the most important structure for the mineralization because of its great scale and wide scope, and it has the most extensive impact in southeastern China (Lv, 2014; Zhang et al., 2011). At the end of the D2 stage, extensional deformation occurs that allow the spaces for intrusions and mineralization. The nappe thrusting had resulted in some recumbent folds dipping NW and a sheared zone along thrust planes in the autochthonous ore formation (C_{2+3}–K_1). The deposit is located in the northwestern limb of the NE trending Makeng anticline complex, and it seemed to be controlled by the NE-NNE striking detachment faults (Fig. 2). The emerging of the diabase in the ore district represents the deformation changes from compression to extension (Zhang, 2012; Zhang et al., 2012a,b). With the large-scale cover nappe structure acting as a good hydrothermal shield, the decollement

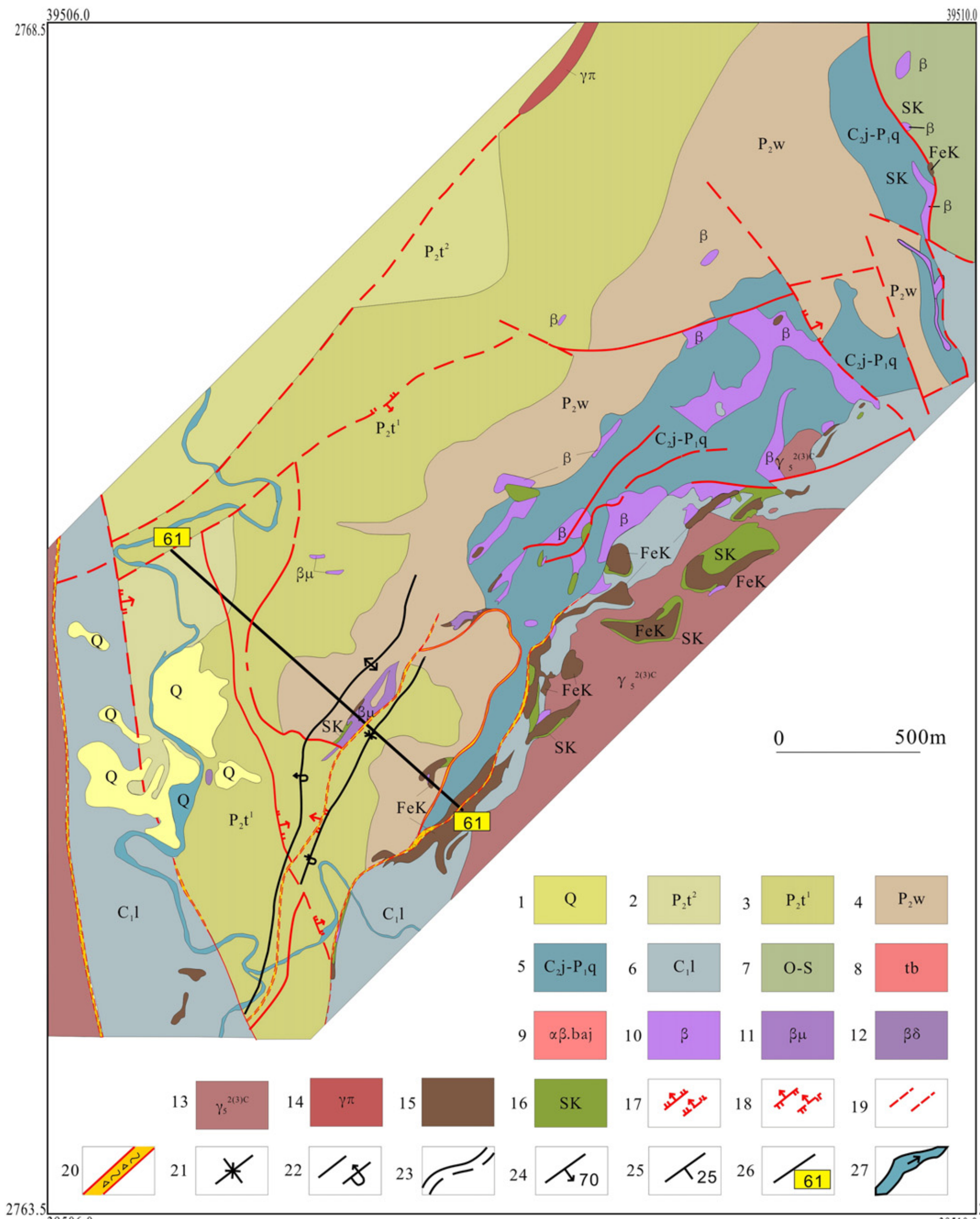

1-Quaternary; 2-The second member of Upper Permian Tongziyan formation; 3-The first member of Upper Permian Tongziyan formation; 4-Upper Permian Wenbishan formation; 5-Upper Carboniferous Jinshe-Lower Permian Qixia formation; 6-Lower Carboniferous Lindi formation; 7-Ordovician Luofengxi formation; 8-Welded tuff breccia (?); 9-Diabase porphyrite; 10-Diabase; 11-Gabbro-diabase; 12-Diabase-diorite; 13-Yanshanian biotite-granite; 14-Granite-porhpyry; 15-Limonite; 16-Skarn; 17-Normal fault; 18-Reverse fault; 19-Unknown fault; 20-Fault fracture zones; 21-Fold axis; 22-Overturened fold axis; 23-Geological boundary; 24-Fault occurence; 25-Attitude of stratum; 26-No. 61 geological section; 27-Rivers; F1-F13 are fault numbers;

Fig. 2. Geological map of the Makeng mine district. After No. 8 Geological Team, Fujian Bureau of Geology (1982).

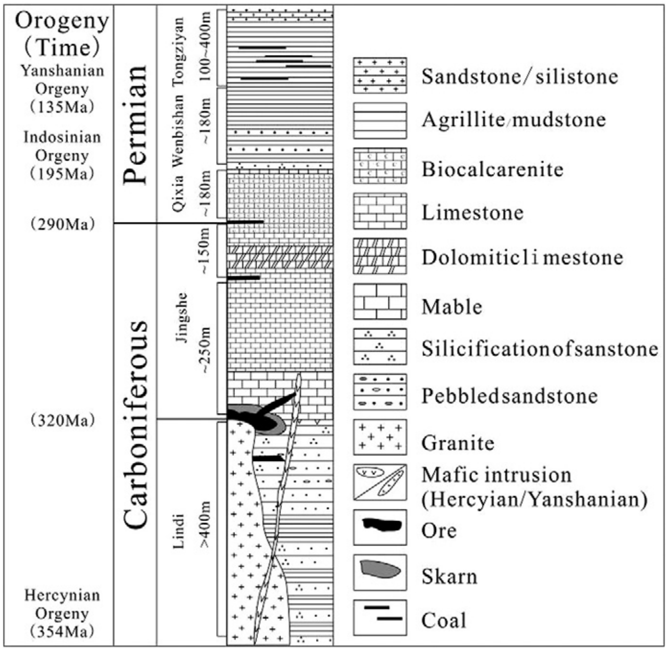

Fig. 3. Stratigraphic section of the Makeng deposit. After Zuo et al. (2015).

provides a space to accommodate fluids derived from the intrusions and sedimentary rocks, thereby forming the Makeng ore deposits. Therefore, the structures, as well as frequent intrusion-induced hydrothermal activities provide a good foundation for mineralization.

3. Geological constraints for ore-forming geodynamics

The Makeng deposit is dominated by the Carboniferous strata, which include the Carboniferous Lindi and Jingshe Formations, and the Permian strata, which include the Qixia, Wenbishan and Tongziyan Formations (Fig. 3).The Lindi formation is composed of a series of continental-marine detrital and pyroclastic rocks, while carbonates make up the Jingshe Formation. The Qixia Formation primarily consists of offshore shallow sea sedimentary and impure limestones. The Wenbishan and Tongziyan Formations are composed of sandstone, argillite, siltstone, mudstone, and shale. A wealth of geochronological data from Chinese literature on the Juzhou–Dayang granite suites, emplaced on both sides of the Makeng Fe–Mo deposit (Fig. 2), suggests two episodes of intrusion. The earlier episode happened in the late Jurassic (145–155 Ma) (Yan, 2013; Zhang, 2012), while the later episode occurred in the Early Cretaceous (125–137 Ma) (Zhang et al., 2012b). Zhang and Zhang (2014) believed that the Juzhou and Dayang intrusions form one batholith at depth because they have similar petrology, mineralogy and geochemical characteristics. Furthermore, similar granite has been observed during core logging of drill cores, which were drilled between the outcrops of the two granite suites. Wang et al. (2010) and Zhang et al. (2012a,b) obtained molybdenite mineralization ages of 130.50 ± 0.92 Ma and 133.0 ± 1.9–134.0 ± 4.2 Ma, respectively, by employing Re–Os isotope geochronology on the molybdenite of the Makeng deposit. Separations of pure garnet skarn alteration and iron mineralization of the Makeng deposit yielded Sm–Nd isochron ages of 157 ± 15 Ma (Zhang et al., 2012a,b), suggesting responses to even earlier intrusions. Hercynian diabase (303 ± 2 Ma, dated by Zhang, 2012) intruded the interface of the limestones of the Carboniferous Jingshe–Permian Qixia Formations which are strongly deformed or altered to skarns. There are also several later Yanshanian

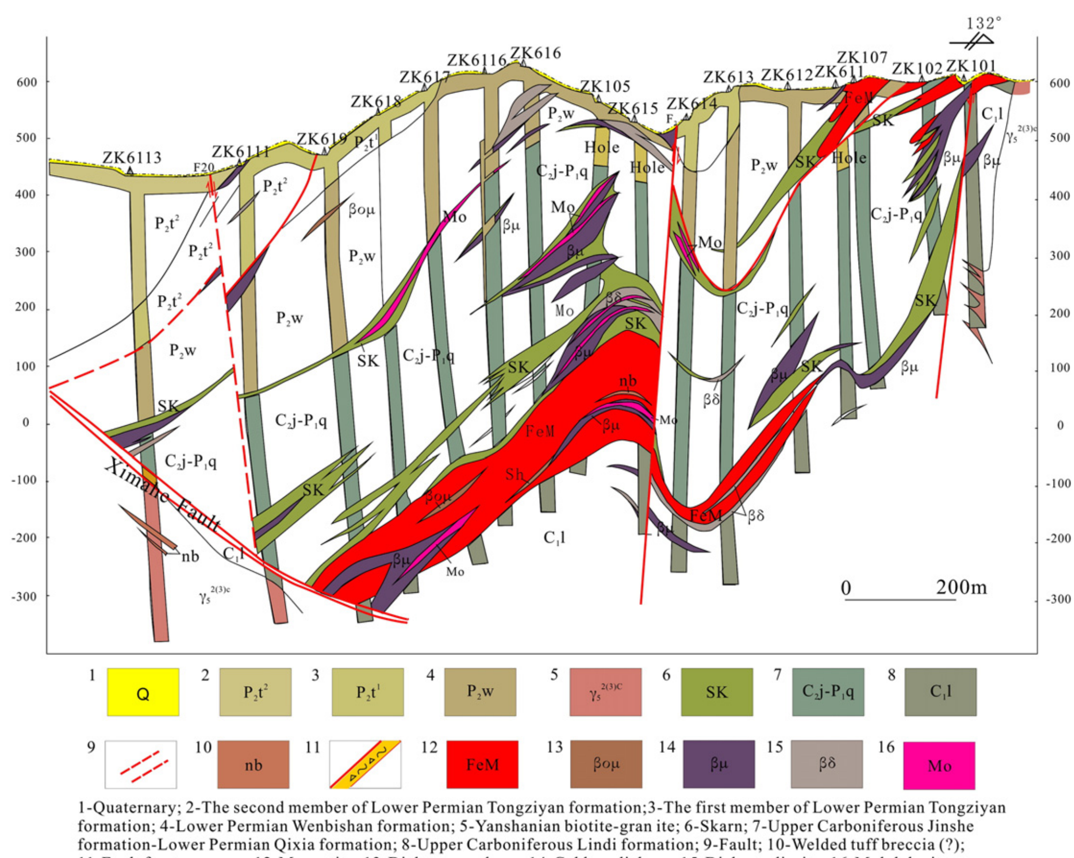

Fig. 4. Geological section for No. 61 prospecting line of the Makeng mine district. After No. 8 Geological Team, Fujian Bureau of Geology (1982).

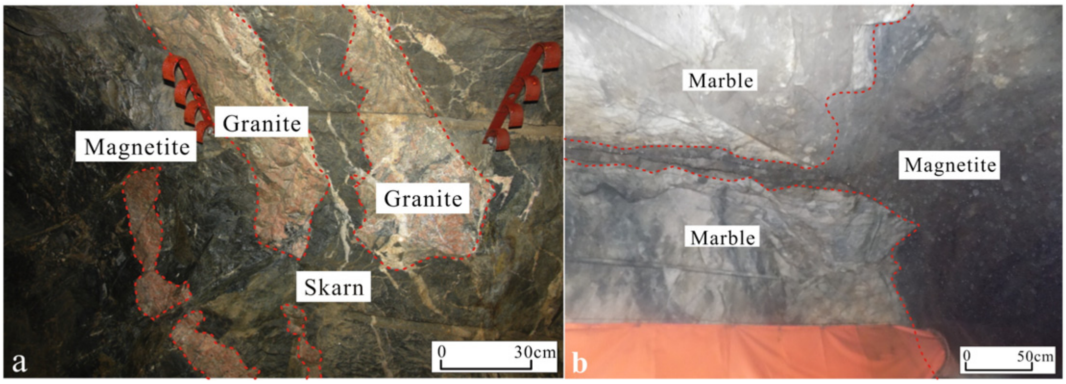

Fig. 5. Granite clasts in or body of the Makeng deposit (a). Offshoots of magnetite ore penetrate into marble and the zigzag boundary of ore body (b).

diabases (64 ± 1 Ma) (Zhang, 2012), which cut the iron ore body. The Juzhou and Dayang intrusions are roughly in the alignment of the NE-NNE basement faults. As a result, the iron mineralization is a response to the widespread intrusions of the early Yanshanian Juzhou–Dayang granite (Zhang, 2012; Zhang and Zuo, 2014). Iron mineralization and alteration are located along the contact between the Lindi Formation sandstone and Jingshe Formation–Qixia Formation carbonate (Fig. 3). In addition, there are nearly 200 little lentoid ore bodies found to be sandwiched between the pairing of Jingshe–Qixia and Qixia–Wenbishan Formations. The main ore body of the Makeng deposit is thickly zoned and distributed along the core of the Makeng anticline with the axial plane dipping NW, while the small scale ore bodies are bedded and lenticular. The ore bodies trend in the NE direction, which is consistent with the strike direction of the wall rock (Fig. 4).

The implications of the geological and geochemical constraints of the Makeng iron deposit on its metallogenesis are:

(1) The regional tectonism regime changed from compressive shortening (napping structures developed) to extensional stretching (decollement developed) (Lv, 2014). Mineralization occurs during the slipping process which was developed under tensional deformation.
(2) Several granite xenoliths are observed within magnetite ore (Fig. 5a), suggesting that the magnetite must have been deposited after the intrusion had solidified during cooling.
(3) Most ore bodies have sharp boundary with the wall rock (marble) with no wall rock alteration. Moreover, several offshoots of magnetite ore penetrate into the wall rock (Fig. 5b). This finding implies that the skarnization process is due to chemical reaction processes, but the ore body formation and localization must have a strong relationship with the mechanical process of the rock, which can form the necessary dilation zone for ore deposition. Moreover, the sharp zigzag ore boundary indicates that dilation zones are induced by tensional stress.
(4) The ore body is structurally controlled by faults that were developed when the regional deformation changed from compressive shortening to extensional stretching approximately 145 to 138 Ma (Lv, 2014), while the cooling ages of the ore-related intrusions are 128.8 to 133.9 Ma (Zhang, 2012; Zhang et al., 2012b). This suggests that the magmatic–hydrothermal system of the Makeng deposit was formed under tensional deformation. The ore body is seldom distributed around the contact zone between the intrusions and wall rock, meanwhile there are many small ore bodies hosted in limestone (Jinshe–Qixia Formation (C_2j–P_1q)) (Fig. 4). It is certain that such an uneven distribution of ore bodies cannot be ascribed solely to differences in chemical composition because there is no such uneven distribution of chemical composition along the entire contact zone. This implies that both the scale and location of the skarn ore bodies are controlled by complex coupled geodynamics that play an important role in the ore forming process, such as temperature, stress, strain and hydrological properties (Zhao et al., 2008a, 2009).
(5) Even though iron ore bodies are definitely associated with skarns (Fig. 4), the relationship between them is highly complex. Yan (2013) observed some flow structure in the skarn and melt inclusions were observed in skarn and wall rocks, which imply that the skarn was developed from a melt. It can be known that the major skarn minerals must be formed before the formation of the iron ore.

4. Computational modeling

4.1. Mathematical description of the numerical modeling

The ore genesis, its localization and geodynamics of the Makeng deposit form a complex metallogenic system. Geodynamic simulation is an effective method to understand the formation of a deposit (Walshe et al., 2001; Hobbs et al., 2006; Zhao et al., 2008a, 2009; Reid et al., 2012a; Poulet et al., 2013; Poulet and Regenauer-Lieb, 2015a,b). The numerical simulation sequence of the geodynamic process is

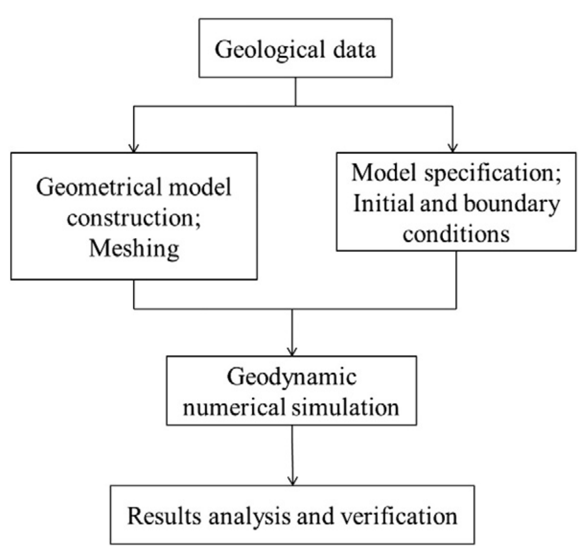

Fig. 6. Numerical simulation of the geodynamic process.

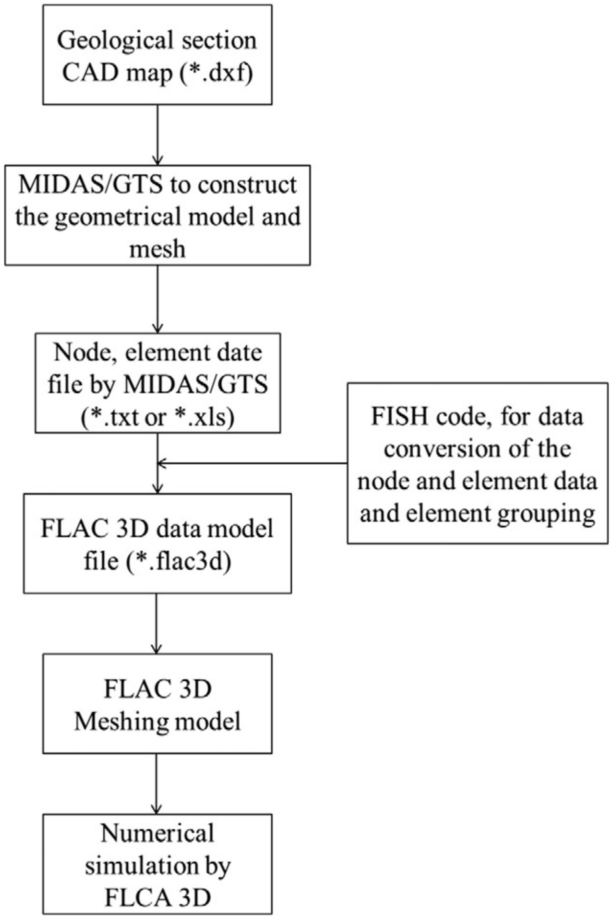

Fig. 7. Workflow of programming for MIDAS/GTS and FLAC3D model conversion.

shown in Fig. 6. In our study, we used the FLAC3D (Fast Lagrangian Analysis of Continua in Three Dimensions) software to simulate the mechano–thermo-hydrological (MTH) processes associated with the cooling of the Juzhou–Dayang intrusion that is spatially related and cogenetic to the Makeng deposit. All mediums are considered to be porous Mohr–Coulomb materials, with mechanical behavior that satisfies the Mohr–Coulomb fracture criteria as summarized in Vermeer (1998) and Mandl (1988). FLAC3D is the three-dimensional explicit finite difference simulation software that is based on the Lagrangian difference method, and it can consider different materials for implementing the corresponding constitutive equations. Using FLAC3D to simulate the mechano–thermo-hydrological processes can truly represent the real material dynamic behavior (Itasca Consulting Group, 2005).

Detailed description of the governing mathematical equations of ore-forming systems is often discussed in many literatures (e.g., Zhao et al., 2008b, 2009; Zhao, 2009, 2014; Reid et al., 2012a). In our FLAC3D models, the coupled geodynamics are governed by the following equations (Liu et al., 2010a,b, 2011, 2012):

$$q_i^f = -\frac{k_{ij}^a}{\mu}\frac{\partial}{\partial x_j}\left(P - \rho_f g_j x_j\right) \tag{1}$$

$$q_i^T = -\left(\phi\lambda_{ij}^f + (1-\phi)\lambda_{ij}^s\right)\frac{\partial T}{\partial x_j} \tag{2}$$

$$\frac{\partial q_i^f}{\partial x_i} = -\frac{\partial \zeta}{\partial t} + q_v^f \tag{3}$$

$$\left(\phi\rho_f C_v^f + (1-\phi)\rho_s C_v^s\right)\frac{\partial T}{\partial t} = -q_i^f\frac{\partial T}{\partial x_i} - \frac{\partial q_i^T}{\partial x_i} + q_v^T \tag{4}$$

$$\rho\frac{d\dot{u}}{dt} = \frac{\partial \sigma_{ij}}{\partial x_j} + \rho g_i \tag{5}$$

$$\frac{\partial \varepsilon_{ij}^T}{\partial t} = \alpha_T\frac{\partial T}{\partial t}\delta_{ij} \tag{6}$$

$$\frac{\partial P}{\partial t} = M\left(\frac{\partial \zeta_H}{\partial t} - \alpha\frac{\partial \varepsilon_v}{\partial t} + \beta\frac{\partial T}{\partial t}\right). \tag{7}$$

Table 1 shows each symbol and its scientific meaning. Eqs. (1) and (2) are the Darcy law describing fluid flow and the Fourier's law describing heat transfer, respectively; Eqs. (3)–(5) describe the conservation of mass, energy and momentum, respectively; and Eqs. (6) and (7) describe the coupled MTH constitutive relations.

4.2. Model construction

To simulate the ore-forming processes of a deposit with complex geodynamics, such as the Makeng deposit, one challenge is the construction of discrete grids that are compatible with the selected software. Because the FLAC3D mainly focuses on dynamic simulations, its functions can be employed by constructing a mesh model for complex bodies, such as those of the Makeng deposit involving irregular intrusions. Thus, considerably more advanced professional software is required to construct discrete grids. In our study, professional modeling tools, namely, Auto CAD and MIDAS/GTS combined with the FISH program, were used to construct the discrete grid model of the Makeng iron deposit metallogenic system. The process is broken into two steps

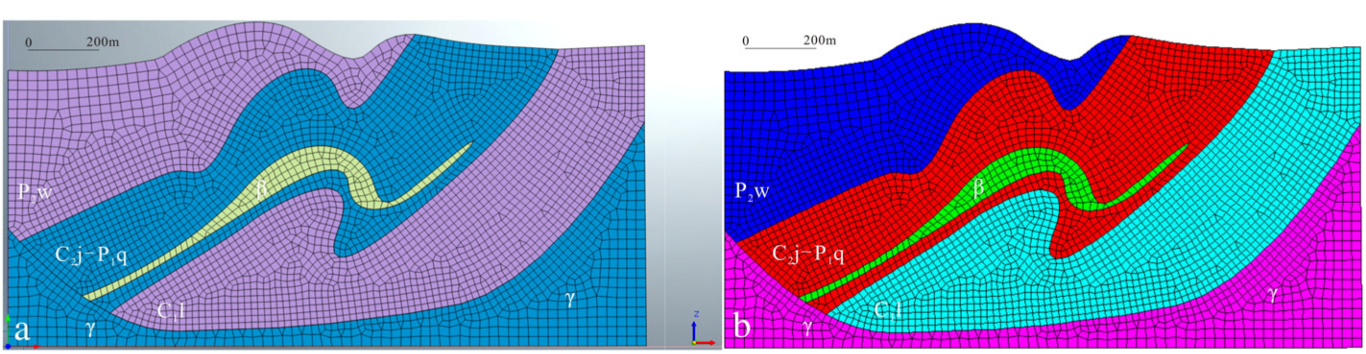

Fig. 8. Geodynamic model constructed by MIDAS/GTS (a); transformed model by the Fish program (b).

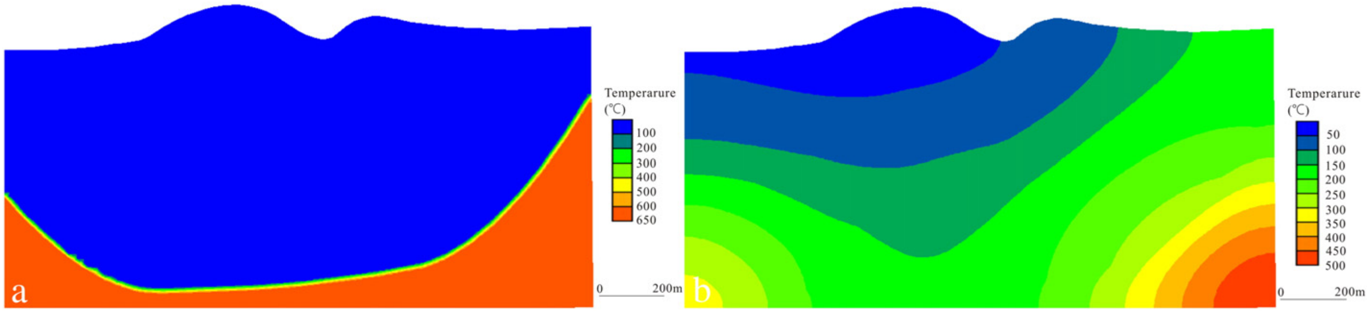

Fig. 9. The temperature distribution of the model at the beginning of the experiment (a) and after the simulation (b).

(Fig. 7): constructing the entity model (mesh model) and conversion of the data format. The effects of the surrounding rocks around the model should be considered using the infinite elements (Zhao, 2009). It is worth noting that due to the limitation of applying FLAC3D on the simulation model, the effect of surrounding rocks were neglected in this study.

Firstly, Auto CAD was used to assign coordinates to each drawing line of the model, then the file (*.dxf format) was export from Auto CAD. Secondly, the model (*.dxf format) was imported into MIDAS/GTS to create the mesh model manually. Thirdly, the element list and node list constructed in MIDAS/GTS were exported into the Excel form. A FISH program was used to rearrange the data and convert it to a format that is compatible with the FLAC3D. Lastly, we imported the model into FLAC3D. The model, which is shown in Fig. 8a, was constructed by MIDAS/GTS. The self-compiled FISH program was used to convert the format and import it into FLAC3D. Fig. 8b shows a complete consistence between the two programs.

The above geodynamic model (Fig. 8) is constructed based on the synthesis of typical sections of the Makeng iron deposit (Fig. 4) to simulate the MTH processes during the syntectonic cooling of the Juzhou–Dayang intrusion. The initial and boundary conditions used in this paper are based on the geological constraints on the geodynamic evolution of the Makeng deposit and regional crust.

4.3. Model setup

4.3.1. Model specification

The hydrological, mechanical and thermal properties employed in the models described in the following sections are tabulated as Table 2. The data were obtained from Itasca Consulting Group (2005) and Schön (1998). These properties depend on the rock type and its petrological composition. In certain rock units, these properties change significantly under different conditions. The data were selected by considering the parameters that have an influence on the properties (in Table 2). We then compare the model results obtained from using different data properties to the geological condition on the ground. The properties that depend on the temperature and pressure, such as permeability, change during deformation, thus an average value was assigned.

4.3.2. Initial and boundary conditions

All units of the model are regarded as Mohr–Coulomb material. The initial temperature of the top surface is set at 27 °C and kept free. The temperature gradient is set at 20 °C/km for the sedimentary section. The temperature of the Juzhou–Dayang intrusion is set at 650 °C. The FLAC3D software can only operate using a single-phase fluid; therefore, all the porous mediums were initially saturated with water. The initial pore–fluid pressure of the rocks is set to be at hydrostatic pressure. The Fournier (1999) general model stipulates that the initial pore–fluid pressure of the intrusion should be set to near lithostatic pressure. The model undertakes a horizontal extensional elastic deformation with a symmetrical boundary velocity of 2.2×10^{-10} ms^{-1} at both sides and parallel to the X direction of the model. The boundaries are insulated against the heat and are impermeable by the fluid. The model's conditions and fracture criteria described above were chosen based on the following evidence:

(1) Due to the limitation of the numerical code, we do not simulate the whole process of the liquid magma intrusion and metallogenic

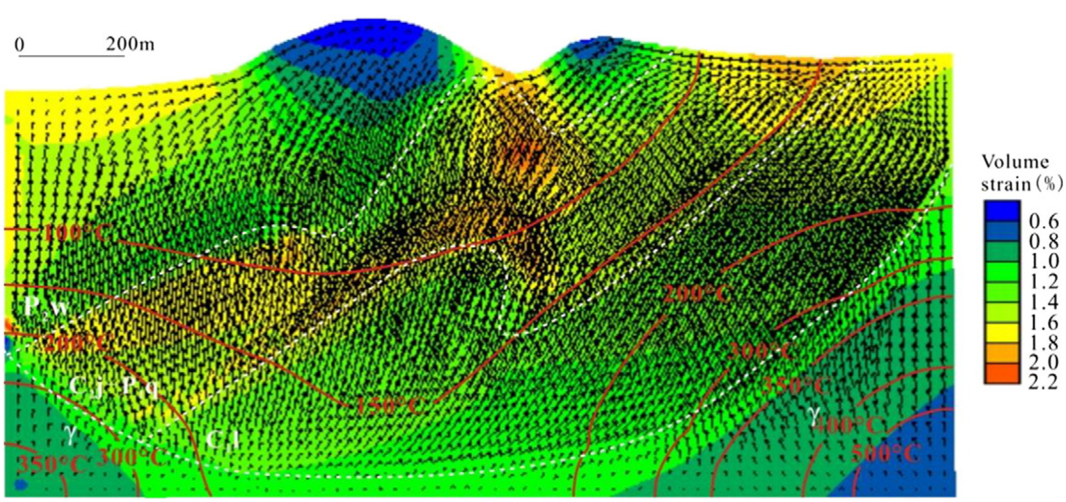

Fig. 10. Deformation, temperature and fluid flow results of the model after the simulation, showing Darcy velocities (arrows), isothermal lines and total volumetric strain contour (the maximum pore–fluid velocity is $1.011e^{-8}$ m/s).

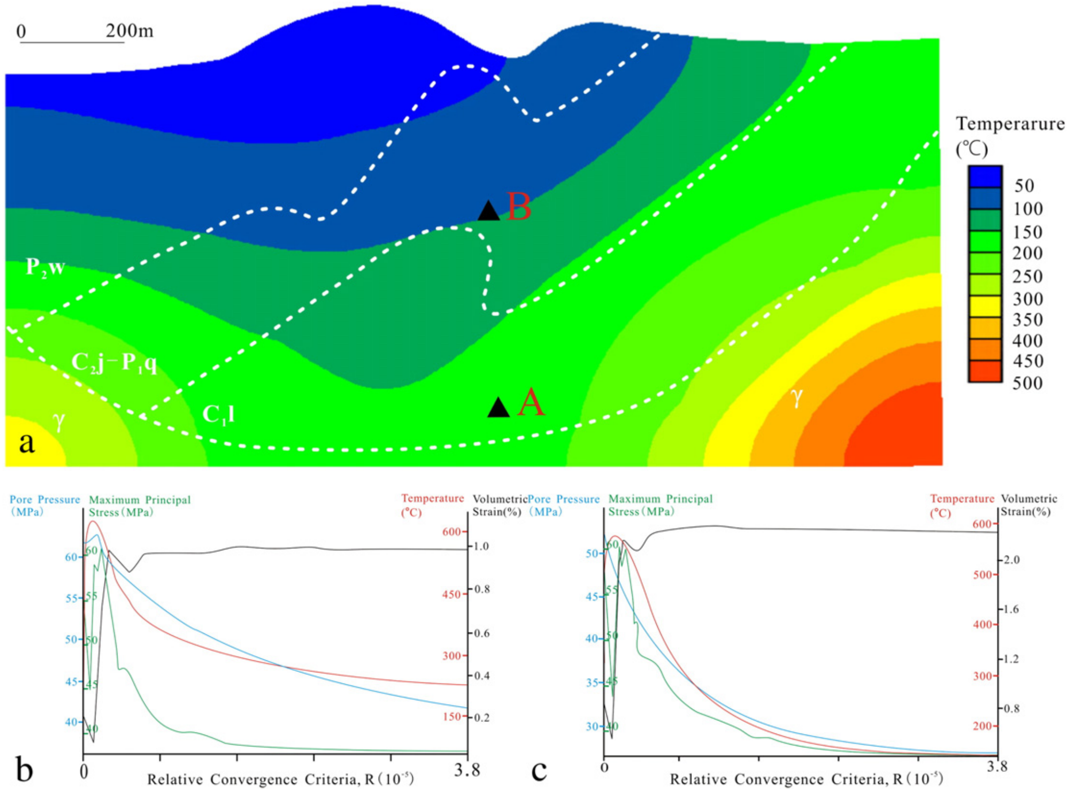

Fig. 11. Temporal variation curves of temperature, pore-fluid pressure, maximum principal stress and volumetric strain increment at different points in the model. (a) Temperature contour in the model, showing the location of points A and B; (b) at point A in the Lindi formation (C_1l) close to intrusion; (c) at point B on the Jinshe Formation (C_2j) close to Lindi. In FLAC, the tensile stress is positive and compressive stress is negative.

evolution, but only the syntectonic cooling processes of the intrusion after solidification, which is largely related to the ore deposition and regarded as the major phase of the mineralization. The model is composed of intrusions and wall rocks, and these units were regarded as viscoelastic porous mediums that meet the Mohr–Coulomb tensile failure criterion.

(2) According to (1), the initial temperature of the intrusion must be lower than the crystallizing temperature of the intrusion and higher than the highest temperature of ore-forming fluids. Qi et al. (1989) established the temperature of intrusion crystallization to be approximately 970 °C. The highest temperature of the ore-forming fluids in the Makeng deposit is 600 °C, which is evaluated by the fluid inclusion (Zhang et al., 2013; Liang and Qu, 1982). Therefore, a temperature of 650 °C is reasonable for the numerical simulation.

(3) Due to the limitation of the FLAC3D software, our numerical experiments only simulate single-phase fluid flow in the porous space. The magma is water-saturated before crystallization. Thus, the initial saturation is set as 1.

(4) During the deformation phase, the regional structure is in the tensional setting (Lv, 2014). Thus, the boundary velocity is 2.2×10^{-10} ms^{-1}. The boundary velocity is a little faster than the stretching velocity of the regional crust during the early Cretaceous (Liu et al., 2011).

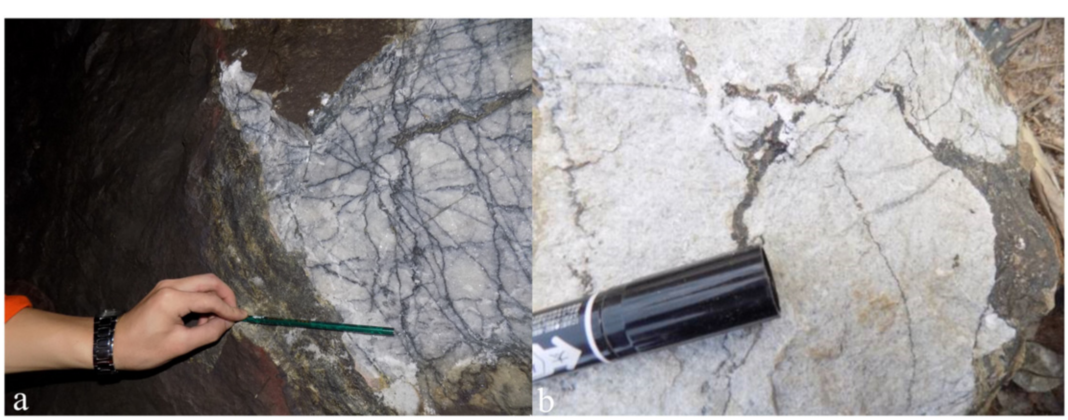

Fig. 12. The magnetite interleave into marble in underground (a), and surface (b).

Fig. 13. Molybdenum hosted in structural fracture in quartz sandstone (Lindi formation).

5. Modeling results, discussion and implication for ore localization and exploration

The above initial and boundary conditions for the FLAC3D model were used to simulate the syn-stretch cooling evolution of the Juzhou–Dayang intrusion. The duration of ore-forming process is unknown, therefore the computational simulation was controlled by the convergence criteria of the FLAC3D code, which stipulate that the ratio (R) of the maximum unbalanced force and the internal force is less than 10^{-5}. The experiment results showed that heat transfer and structural constraints have significant effects on the deformation and pore–fluid flow during the cooling processes of the intrusion after solidification. The results are highly useful for analyzing the location and the fluid flow and in selecting targets for the deep-ore exploration in this ore field.

5.1. Spatial and temporal distribution of temperature

The cooling process of the intrusion after it solidifies influences the change in temperature. The simulation experiment shows the distribution of the temperature in time and space. The initial temperature of the intrusion was set as 650 °C, and the temperature of the wall rocks was controlled by the temperature gradient (Fig. 9a). The simulated model demonstrated that the temperature of the intrusion has a very complex spatial variation (Fig. 10b). The majority of the intrusion's temperature and its surroundings decreased to lower than 250 °C, but some specific places remained higher than 350 °C. Such a variation of the temperature has a direct relationship with the intrusion. Remarkably, it is observed that the existing ore bodies are localized on or close to the places that maintained high temperatures over time.

5.2. Flow-focusing dilation and the mechanisms of ore deposition

The most distinct feature of the model is the heterogeneous distribution of the deformation and pore–fluid flow. The effect of temperature on hydrological and mechanical behaviors of the rock units may cause tensile failure along the contact of the intrusion where there is no boundary velocity. Initially, the dilation deformation may be in micro-strain, and the pore–fluid flow is mainly from the intrusion to the host rocks (Liu et al., 2011). The temperature has an influence on the deformation to a certain extent, with the most important factor possibly being the decollement with a boundary velocity.

Under stress, it is afterward observed from the simulated model that most of the dilation deformation space is strictly distributed along the carbonates of the Jinshe–Qixia Formation (C_2j–P_1q), and as a result the contact between the Lindi formation (C_1l) and Jinshe–Qixia Formation (C_2j–P_1q) becomes more dilated. The pore–fluids are more likely to be pressured into these weak zones and thus cause the occurrence of mineralization (Hobbs et al., 2000, 2004; Zhao et al., 2008a, 2009; Zhao, 2014, 2015). Previous researchers (Chen, 2010; Gao et al., 1985; Luo and Yan, 1980) observed that the interface between the Lindi formation (C_1l) and Jinshe–Qixia Formation (C_2j–P_1q) is the main ore-hosting zone in the Makeng iron deposit. Comparing Fig. 10 to Fig. 4, it is observed that no ore body has been discovered in the Wenbishan Formation (P_2w) and Lindi Formation (C_1l), where no conspicuous deformation induced dilation was observed in the model. This phenomenon pinpoints the importance of the deformation-induced dilation to the ore formation and localization. The most deformation-induced dilation is observed at the crests of anticlines (Fig. 10). These dilatant deformation spaces are more likely to be the focusing center of the pore–fluids coming from the magmatic intrusion and sedimentary rock. However, it can be seen from the simulation model (Fig. 10) that the Lindi formation (C_1l) is also a flow focusing strata because the quartz sandstone has a high permeability; thus, it is easier for fluid to flow, but it is not mineralized. This means that some other factors, such as the physio-chemical conditions and chemical reactions (Hobbs et al., 2010a,b, 2011; Ord et al., 2008a, 2013a,b; Zhao et al., 2012, 2013; Zhao, 2014), have a major role in the ore deposition. In our study we consider that the change in temperature played a role in ore formation when the physico-chemical conditions are favorable.

As the temperature of the intrusion decreases, those of the wall rocks increase. Different points in the model show different distributions and temperature gradients that have nonlinear relationships with

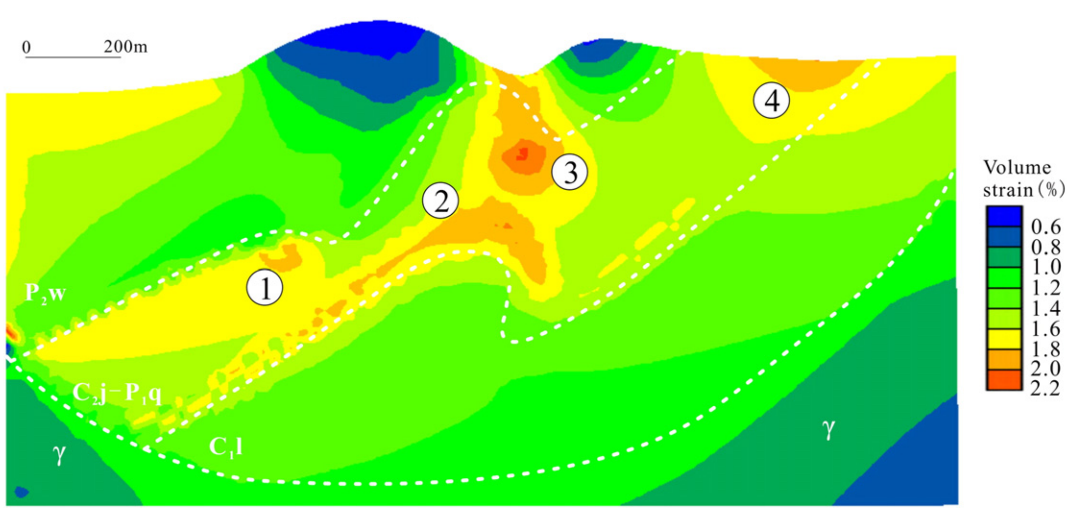

Fig. 14. The prediction targets for computational modeling, which is identical to previous exploration.

time (Fig. 11). Theoretically, the change in temperature may lead to an increment of pore–fluid pressure and stress due to thermal expansion of pore-fluids and solids. Our simulation model shows a very complex relationship between the temperature, volumetric strain increment, pore–fluid pressure, and the maximum principal stress. We chose two points (Fig. 11a) in the Lindi Formation (C_1l) and Jinshe–Qixia Formation (C_2j–P_1q) to investigate the relationship between the temperature, volumetric strain increment, pore–fluid pressure and the maximum principal stress. It shows an arbitral relationship between the two. At point A (in the Lindi Formation (C_1l)), the temperature and pore–fluid pressure decrease slowly, while the volumetric strain increases slowly (Fig. 11b), as well. At point B (in the Jinshe–Qixia Formation (C_2j–P_1q)), the temperature and pore–fluid pressure decrease rapidly, while the volumetric strain increases rapidly (Fig. 11c). Thus, the fastest decrease in temperature gradient and pore–fluid pressure is within the Jinshe–Qixia Formation (C_2j–P_1q) (limestone); additionally, according to the theory of modern mineralization proposed by Zhao et al. (2008b, 2009), the conditions described above are most favorable for ore localization. The results imply that a rapid decrease in temperature and pore–fluid pressure, coupled with rapid increase in volumetric strain, give the Jinshe–Qixia Formation (C_2j–P_1q) a favorable condition to host ore bodies. The maximum principal stress begins with a drastic increase and later falls arbitrarily. In FLAC3D, the tensile stress is positive, while compressive stress is negative. During the decollement, rocks are in tensile stress, negative pore–fluid flow decreases the pore–fluid pressure, so that the maximum principal stress becomes high, which eventually leads to rock failure. This eliminates the influence of pore–fluid pressure and leads to the increase in tensile stress, thus the maximum principal stress decreases. This can facilitate the formation of ore-hosting space and thus the mineralization. The deformation-induced dilatant, pore-fluid flow focusing, as well as pore–fluid pressure variation, are also closely associated with the Juzhou–Dayang intrusion, suggesting that the Juzhou–Dayang magmatic intrusion and the mechanical property of materials of different formations are important constraints on the ore formation and localization.

5.3. Implication for ore localization and deep/periphery exploration

The modeling experiment results show that there are major dilation spaces in which the ore bodies are mostly localized, suggesting that these zones exhibit a great potential for finding undiscovered ore bodies. The existing ore deposits, which have a close spatial association with the dilation zones, are attributed to the deformation-induced dilation. Essentially, the fluid flow flux was accommodated, so it is possible that ores can be deposited. The tonnage and grade of the ore body are positively related to the dilatant deformation; this suggests that dilation deformation may control the pore-fluid flow pattern related to mineralization. Thus, deep exploration should target dilation spaces. This indicates that the dilatant deformation generated by the coupled mechano-thermo-hydrological (MTH) processes during the syn-stretching cooling of the intrusion is a critical factor for controlling ore formation. The mixing of different sources of pore-fluids may be the mechanism for the deposition of ores. The focusing and mixing fluids is generally an effective mechanism for the deposition and localization of hydrothermal ores (Zhao et al., 2008a, 2009). The fluid inclusion and isotopic geochemistry study of the Makeng deposit (Zhang et al., 2013) showed that phase separation of magmatic water and fluid mixing with meteoric water as well as buck boiling might have been the main factors responsible for mineralization, except for some contributions made by other factors such as wall rocks.

5.4. Periphery area geological phenomenon and other evidence

Interesting phenomena occurred in the Makeng deposit, such as the magnetite interfingering into the marble (Fig. 12a). On the surface, we also found the same geological phenomenon (Fig. 12b), indicating that the pore-fluid with high pressure flows into the cracks and makes it dilatant as a shear fracture. In addition, differential stress plays an important role in the rock fracture. A large stress difference could lead to a shear fracture (Sibson, 2004). Liu et al. (2010b) studied constraints of the tectonic stress regime on the mineralization system and showed that it is more easy to develop a skarn deposit with a large stress difference. Zhang et al. (2011) investigated the evolution of a tectonic stress field in the southwestern Wuyishan Mountain area and calculated the maximum and minimum principal stress, which were in a large differential stress. Thus, this large differential stress favored the mineralization of the Makeng deposit. As it was discussed before, there was no conspicuous dilatant deformation developed in the Wenbishan (P_2w) and Lindi (C_1l) formations; therefore, there were no iron ore bodies found in the two sedimentary formations. However, with the higher permeability and porosity, the ore-forming fluids are more likely to percolate and be restored. This explains the molybdenum mineralization observed in the structural fractures of the Lindi Formation (Fig. 13) and pinpoints the importance of the dilation deformation to ore formation and localization. Thus, for the Makeng deposit, further exploration should target the deep dilation zone between the Wenbishan (P_2w) and Jinshe–Qixia (C_2j–P_1q) formations. Indeed, the computational model shows the same depth as found through deep geological drilling, which also discovered significant ore bodies (Figs. 4 and 14). Ferritization and skarn have also been observed during core logging of drill cores and outcrop, indicating the possibility of discovering a new ore body. This finding demonstrates that computational geodynamic modeling can facilitate the selection of the targets for further mineral exploration.

6. Conclusions

The computational geodynamic model experiment results indicate that the large dilation space produced by the coupled MTH process controls the localization and scale of the iron ore body. The dilatant deformation may produce a high porosity space. This space becomes the focus and trap for magmatic and meteoric fluids. Pore-fluid mixing within the carbonate strata creates the right physio-chemical conditions for metals to precipitate as the temperature decreases such that an ore body can be formed. Through FISH programming, the complex geological model was transformed from MIDAS/GTS to FLAC3D to simulate the syntectonic cooling processes of the Juzhou–Dayang intrusion. The modeling results proved the usefulness of using such an emerging computational geoscience method for the cognition of: (1) the movement and focusing of mineral liquid; (2) the volumetric strain increment of the intrusion; and (3) the formations and relationship between them, which fully present the physical mineralization process of the Makeng iron deposit. The mechanical properties of rock are important factors for controlling ore, and the structural fracture of the Lindi formation is the space of an ore deposit. This provides some basis for facilitating predictive discovery of concealed orebodies. However, due to the limitation of the FLAC3D, the related geochemical processes that can play an important role in ore body formation and mineralization (Zhao et al., 2010, 2012, 2013; Zhao, 2014) have been neglected in this study. To determine the ore-forming dynamics in the Makeng ore district, this issue should be considered for future research.

Acknowledgments

This work was jointly supported by the Key Project of Natural Science Foundation of China (grant no. 41530321); the Program of Integrated Prediction of Mineral Resources in Covered Areas (grant no. 12120113089600) and the Fundamental Geological Research on Fully Equipped Areas (grant no. 12120114028701) from the China Geological Survey. We acknowledge Fujian Makeng Mining Co., Ltd. for the support in the field investigation. Special thanks are given to the anonymous reviewers for their valuable comments on our early version of this paper.

Appendix A

Table 1
Symbols and their scientific meanings in equations.

Symbol	Scientific meanings
q_i^f	The fluid specific discharge vector
q_i^f	The heat-flux vector
k_{ij}^a	The apparent mobility coefficient being a function of permeability (k_{ij}) and saturation (s) as $k_{ij}^a = k_{ij}s^2(3-2s)$
μ	The dynamic viscosity of the pore fluid
P	The pressure of the pore fluid
λ_{ij}^f	The thermal conductivity tensors of the fluid
λ_{ij}^s	The thermal conductivity tensors of the solid
T	The temperature
ρ_s	The densities of the solid
ρ_f	The densities of the fluid
g_j	The component of gravitational acceleration in the x_j direction
ζ	The variation of fluid volume per unit volume of the porous material
q_v^f	The volumetric fluid source
q_v^T	The volumetric thermal source
C_v^f	The specific heats of the fluid
C_v^s	The specific heats of the solid
σ_{ij}	The stress tensor of the solid
ρ	$\rho = (1-\phi)\rho_s + \phi\rho_f$, the bulk density of the porous medium
ϕ	The porosity
$\dot{\mu}_i$	The velocity component in the x_i direction
ε_{ij}^T	The thermal strain tensor
ζ_H	The variation of fluid content
ε_v	The volumetric strain
M	The Biot modulus
δ_{ij}	The Kronecker delta
α	The Biot coefficient
β	The volumetric thermal expansion coefficient

Table 2
Parameters of the model.

Model unit	Main lithological composition	Density (kg/m^3)	Bulk modulus (10^{10} Pa)	Shear modulus (10^6 Pa)	Tensile strength (10^6 Pa)	Cohesion (10^6 Pa)	Friction angle (°)	Dilation angle (°)	Permeability (10^{-12} m^2)	Porosity	Thermal conductivity (W·m^{-1}·k^{-1})
P_2w	Silty mudstone	2530	2.15	0.92	2.0	3.4	25	5	9	0.22	4.2
C_2j–P_1q	Micrite limestone	2580	3.2	2.1	2.3	4.2	10	18	20	0.15	2.5
C_1l	Quartz sandstone	2560	3.0	1.8	2.2	3.8	32	4	28	0.25	1.9
Early intrusion	Diabase	3000	2.65	1.97	2.4	3.9	55	8	40[a]	0.2	2.0
Intrusion	Granite	2670	3.63	2.2	1.42	3.4	35	4	8.5	0.12	1.8

[a] Due to the fact that the diabase was deformed by the late reformation, its permeability changed.

References

Alt-Epping, P., Zhao, B.C., 2010. Reactive mass transport modeling of a three-dimensional vertical fault zone with a finger-like convective flow regime. J. Geochem. Explor. 106, 8–23.

Awadh, S.M., Ali, K.K., Alazzawi, A.T., 2013. Geochemical exploration using surveys of spring water, hydrocarbon and gas seepage, and geobotany for determining the surface extension of Abu-Jir Fault Zone in Iraq: a new way for determining geometrical shapes of computational simulation models. J. Geochem. Explor. 124, 218–229.

Charifo, G., Almeida, J.A., Ferreira, A., 2013. Managing borehole samples of unequal lengths to construct a high-resolution mining model of mineral grades zoned by geological units. J. Geochem. Explor. 132, 209–223.

Chen, Y., 2002. New knowledge of the information cause of ore deposit during the exploitation process of Makeng Iron Mine. Met. Mine 317, 50–52 (in Chinese with English Abstract).

Chen, Y., 2010. New understanding of ore–control structure feature of Fujian Makeng iron mine. Met. Mine 2, 96–99 (in Chinese with English Abstract).

Chen, S., Xie, J., Xu, C., Guo, W., 1985. The origin of Makeng Iron Deposit, Fujian. Geochimica 4, 350–357 (in Chinese).

Di, Y., Zhang, D., Wu, G., Yan, P., Lai, S., Gong, Y., 2012. Strata hosted making type iron deposits and prospecting orientation in the Wuyishan covered region. Earth Sci. J. China Univ. Geosci. 37 (6), 1232–1242 (in Chinese with English Abstract).

Eldursi, K., Branquet, Y., Guillou-Frottier, L., Marcoux, E., 2008. Numerical investigation of transient hydrothermal processes around intrusions: heat-transfer and fluid circulation controlled mineralization patterns. Earth Planet. Lett. 288, 70–83.

Fournier, R.O., 1999. Hydrothermal processes related to movement of fluid from plastic into brittle rock in the magmatic–epithermal environment. Econ. Geol. 94, 1193–1211.

Gao, L., Zhu, X., Wang, S., 1985. The Late Paleozoic rocks in southwestern Fujian and the ore-controlling horizons of the Makeng-type iron-ore deposits. Bull. Chin. Acad. Geol. Sci. 12, 21–32 (in Chinese with English Abstract).

Garven, G., Freeze, R.A., 1984. Theoretical analysis of the role of groundwater flow in the formation of stratabound ore deposits: 1. Mathematical and numerical models. Am. J. Sci. 284, 1085–1124.

Ge, C., Han, F., Zhou, T., Chen, D., 1981. Geological characteristics of the Makeng Iron Deposit of marine volcano-sedimentary origin. Bull. Chin. Acad. Geol. Sci. 3, 47–69 (in Chinese with English Abstract).

Gow, P.A., Upton, P., Hill, K.C., 2002. Copper-gold mineralization in New Guinea: numerical modelling of collision, fluid flow and intrusion-related hydrothermal systems. Aust. J. Earth Sci. 49, 753–771.

Hobbs, B.E., Zhang, Y.H., Ord, A., 2000. Application of coupled deformation, fluid flow, thermal and chemical modeling to predictive mineral exploration. J. Geochem. Explor. 69-70, 505–509.

Hobbs, B.E., Ord, A., Peng, S., Mühlhaus, H.B., Liu, L., 2004. Theoretical investigation of convective instability in inclined and fluid-saturated three-dimensional fault zones. Tectonophysics 387, 47–64.

Hobbs, B.E., Ord, A., Kuhn, M., Mühlhaus, H.B., Peng, S., 2006. Numerical simulation of double-diffusion driven convective flow and rock alteration in three-dimensional fluid-saturated geological fault zones. Comput. Methods Appl. Mech. Eng. 195, 2816–2840.

Hobbs, B.E., Ord, A., Hornby, P., Peng, S., Liu, L., 2007. Mineral precipitation associated with vertical fault zones: the interaction of solute advection, diffusion and chemical kinetics. Geofluids 7, 3–18.

Hobbs, B.E., Ord, A., Hornby, P., Peng, S., 2008. Effect of reactive surface areas associated with different particle shapes on chemical–dissolution front instability in fluid-saturated porous rocks. Transp. Porous Media 73, 75–94.
Hobbs, B.E., Ord, A., Peng, S., 2010a. Effects of mineral dissolution ratios on chemical–dissolution front instability in fluid-saturated porous rocks. Transp. Porous Media 82, 317–335.
Hobbs, B.E., Ord, A., Zhao, B.C., 2010b. Theoretical analyses of the effects of solute dispersion on chemical–dissolution front instability in fluid-saturated porous rocks. Transp. Porous Media 84, 629–653.
Hobbs, B.E., Regenauer-Lieb, K., Ord, A., 2011. Computational simulation for the morphological evolution of nonaqueous-phase-liquid dissolution fronts in two-dimensional fluid-saturated porous media. Comput. Geosci. 15, 167–183.
Hornby, P., Ord, A., Peng, S., 2006a. Numerical modelling of fluids mixing, heat transfer and non-equilibrium redox chemical reactions in fluid saturated porous rocks. Int. J. Numer. Methods Eng. 66, 1061–1078.
Hornby, P., Peng, S., Liu, L., 2006b. Theoretical and numerical analyses of pore-fluid flow patterns around and within inclined large cracks and faults. Geophys. J. Int. 166, 970–988.
Hornby, P., Ord, A., Peng, S., Liu, L., 2008. Theoretical and numerical analyses of chemical–dissolution front instability in fluid-saturated porous rocks. Int. J. Numer. Anal. Methods Geomech. 32, 1107–1130.
Itasca Consulting Group, 2005. FLAC3D User's Guide. Itasca Consulting Group, INC., Minneapolis.
Jiang, Y., 2009. Analysis of metallogenic geological features in Makeng Iron Deposit. Mod. Min. 8, 89–91 (in Chinese).
Ju, M., Dai, T., Yang, J., 2011. Finite element modeling of pore-fluid flow in the Dachang ore district, Guangxi, China: implications for hydrothermal mineralization. Geosci. Front. 2 (3), 463–474.
Lei, X., Chen, Y., Zhao, J., 2013. Three-dimensional thermo-mechanical modeling of the Cenozoic uplift of the Tianshan mountains driven tectonically by the Pamir and Tarim. J. Asian Earth Sci. 62, 797–811.
Liang, X., Qu, G., 1982. A preliminary experiment on the formation temperature and pressure of the iron deposit in Makeng, Fujian. Bull. Chin. Acad. Geol. Sci. 4, 83–94 (in Chinese with English Abstract).
Lin, Z., 2008. Discussion on geological features and prospecting direction of Makeng Iron Deposit. Express Inf. Min. Ind. 10, 84–86 (in Chinese).
Lin, G., Hobbs, B.E., Wang, Y., Mühlhaus, H.B., Ord, A., 2002. Finite element modeling of reactive fluids mixing and mineralization in pore-fluid saturated hydrothermal/sedimentary basins. Eng. Comput. 19, 364–385.
Lin, G., Hobbs, B.E., Ord, A., Mühlhaus, H.B., 2003. Theoretical and numerical analyses of convective instability in porous media with temperature-dependent viscosity. Commun. Numer. Methods Eng. 19, 787–799.
Lin, G., Zhou, Y., Wei, X., 2006. Structural controls on fluid flow and related mineralization in the Xiangshan uranium deposit, Southern China. J. Geochem. Explor. 89, 231–234.
Liu, L., Yang, G.H., Peng, S.L., 2005. Numerical modeling of coupled geodynamical processes and its role in facilitating predictive ore discovery: an example from Tongling, China. Resour. Geol. 55 (1), 21–31.
Liu, L., Zhao, Y., Zhao, B.C., 2010a. Coupled geodynamics in the formation of Cu skarn deposit in Tongling–Anqing district, China: computational modeling and implications for exploration. J. Geochem. Explor. 106, 146–155.
Liu, L., Zhou, R., Zhao, B.C., 2010b. Constraints of tectonic stress regime on mineralization system related to the hypabyssal intrusion: implication from the computational modeling experiments on the geodynamics during cooling process of the Yuenshan intrusion in Anqing district, China. Acta Petrol. Sin. 26 (9), 2869–2878 (in Chinese with English Abstract).
Liu, L., Wan, C., Zhao, Y., 2011. Geodynamic constraints on orebody localization in the Anqing orefield, China: computational modeling and facilitating predictive exploration of deep deposits. Ore Geol. Rev. 43, 249–263.
Liu, L., Zhao, Y., Sun, T., 2012. 3D computational shape- and cooling process-modeling of magmatic intrusion and its implication for genesis and exploration of intrusion-related ore deposits: an example from the Yueshan intrusion in Anqing, China. Tectonophysics 526-529, 110–123.
Liu, L., Sun, T., Zhou, R., 2014. Epigenetic genesis and magmatic intrusion's control on the Dongguashan stratabound Cu–Au deposit, Tongling, China: evidence from field geology and numerical modeling. J. Geochem. Explor. 144, 97–114.
Luo, J., Yan, Q., 1980. On the horizon and the age of main seam of Makeng type iron deposits in southwestern Fujian. Sci. Geol. Sin. 4, 331–339 (in Chinese with English Abstract).
Lv, L., 2014. Discussions on features of Mesozoic thrust-fault belts and relationship between thrust-fault belts and magmatism in southwestern Fujian and adjacent regions (Ph.D. Dissertation), China University of Geosciences (Beijing), Beijing (in Chinese with English Abstract).
Mandl, G., 1988. Mechanics of tectonic faulting. Int. J. Numer. Anal. Methods Geomech. 13 (3), 339.
No.8 Geological Team, Fujian Bureau of Geology, 1982. The geological features of the Makeng (Longyan, Fujian Province) iron ore deposit and the discussion on its origin. Geol. Fujian (1), 2–31 (in Chinese with English abstract).
Ord, A., Hobbs, B.E., Zhang, Y., Broadbent, G.C., Brown, M., Willetts, G., 2002. Geodynamic modeling of the Century deposit, Mt Isa Province, Queensland. Aust. J. Earth Sci. 49, 1011–1039.
Ord, A., Hornby, P., Peng, S., 2008a. Morphological evolution of three-dimensional chemical dissolution front in fluid-saturated porous media: a numerical simulation approach. Geofluids 8, 113–127.
Ord, A., Peng, S., Liu, L., 2008b. Inversely-mapped analytical solutions for flow patterns around and within inclined elliptic inclusions in fluid-saturated rocks. Math. Geosci. 40, 179–197.
Ord, A., Hobbs, E.B., Zhao, B.C., 2010. Theoretical and numerical investigation into roles of geofluid flow in ore forming systems: integrated mass conservation and generic model approach. J. Geochem. Explor. 106, 251–260.
Ord, A., Hobbs, E.B., Zhao, B.C., 2012. Effects of domain shapes on the morphological evolution of nonaqueous-phase-liquid dissolution fronts in fluid-saturated porous media. J. Contam. Hydrol. 138-139, 123–140.
Ord, A., Hobbs, E.B., Zhao, B.C., 2013a. Analytical solutions of nonaqueous-phase-liquid dissolution problems associated with radial flow in fluid-saturated porous media. J. Hydrol. 494, 96–106 (2013).
Ord, A., Hobbs, E.B., Zhao, B.C., 2013b. Effects of medium permeability anisotropy on chemical–dissolution front instability in fluid-saturated porous rocks. Transp. Porous Media 99, 119–143 (2013).
Peng, S., Ord, A., Hobbs, B.E., Zhao, B.C., 2008. Particle simulation of spontaneous crack generation associated with the laccolithic type of magma intrusion processes. Int. J. Numer. Methods Eng. 75, 1172–1193.
Peng, S., Liu, L., Ord, A., 2011. Computational simulation of convective flow in the earth's crust with consideration of dynamic crust–mantle interactions. J. Cent. S. Univ. Technol. 18, 2080–2084.
Poulet, T., Regenauer-Lieb, K., 2015a. Numerical modeling of toxic nonaqueous-phase-liquid removal from contaminated groundwater systems: mesh effect and discretization error estimation. Int. J. Numer. Anal. Methods Geomech. 39, 571–593.
Poulet, T., Regenauer-Lieb, K., 2015b. Replacement of annular domain with trapezoidal domain in computational modeling of nonaqueous-phase-liquid dissolution-front propagation problems. J. Cent. South Univ. 22, 1841–1846.
Poulet, T., Regenauer-Lieb, K., Hobbs, B.E., 2013. Computational modeling of moving interfaces between fluid and porous medium domains. Comput. Geosci. 17, 151–166.
Price, G.P., Stoker, P., 2002. Australian Geodynamics Cooperative Research Center's integrated research program delivers a new minerals exploration strategy for industry. Aust. J. Earth Sci. 49, 595–600.
Qi, R., Wu, Z., Zou, Y., Fen, Z., Huang, S., Xu, M., 1989. Continental facies polycycle bimodal volcanics along southeastern coast of China. Bull. Chin. Acad. Geol. Sci. 10 (3), 4–23 (in Chinese with Englishabstract).
Reid, L.B., Regenauer-Lieb, K., Poulet, T., 2012a. A porosity-gradient replacement approach for computational simulation of chemical–dissolution front propagation in fluid-saturated porous media including pore-fluid compressibility. Comput. Geosci. 16, 735–755.
Reid, L.B., Regenauer-Lieb, K., Zhao, B.C., 2012b. Some fundamental issues in computational hydrodynamics of mineralization. J. Geochem. Explor. 112, 21–34.
Schaubs, P., Zhao, B.C., 2002. Numerical modelling of gold-deposit formation in the Bendigo–Ballarat zone, Victoria. Aust. J. Earth Sci. 49, 1077–1096.
Schmidt Mumm, A., Brugger, J., Schacht, U., 2010. Fluids in geological processes—the present state and future outlook. J. Geochem. Explor. 106, 1–7.
Schön, J.H., 1998. Physical Properties of Rocks: Fundamentals and Principles of Petrophysics. Elsevier, Oxford.
Sheldon, H., 2009. Simulation of magmatic and metamorphic fluid production coupled with deformation, fluid flow and heat transport. Comput. Geosci. 35, 2275–2281.
Sibson, R.H., 2004. Controls on maximum fluid overpressure defining conditions for mesozonal mineralization. J. Struct. Geol. 26, 1127–1136.
Sorjonen-Ward, P., Zhang, Y., Zhao, B.C., 2002. Numerical modelling of orogenic processes and mineralization in the South Eastern part of the Yilgarn Craton, Western Australia. Aust. J. Earth Sci. 49, 935–964.
Vermeer, P.A., 1998. Non-associated plasticity for soils, concrete and rock. Phys. Dry Granul. Media 350, 163–196.
Walshe, J.L., Mühlhaus, H.B., Ord, A., 2001. Finite element modelling of fluid–rock interaction problems in pore-fluid saturated hydrothermal/sedimentary basins. Comput. Methods Appl. Mech. Eng. 190, 2277–2293.
Wang, W., Ji, S., Xing, W., Wang, R., 1981. A discussion on genesis of Makeng type iron deposit in Southwestern Fujian. Bull. Chin. Acad. Geol. Sci. 2, 1–28 (in Chinese with English Abstract).
Wang, D., Chen, Z., Chen, Y., Tang, J., Li, J., Ying, L., Wang, C., Liu, S., Li, L., Qin, Y., Li, H., Qu, W., Wang, Y., Chen, W., Zhang, Y., 2010. New data of the rock-forming and ore-forming chronology for China's important mineral resources areas. Acta Geol. Sin. 84 (7), 1030–1040 (in Chinese with English Abstract).
Wang, H., Cheng, Q., Zuo, R., 2015. Spatial characteristics of geochemical patterns related to Fe mineralization in the southwestern Fujian province (China). J. Geochem. Explor. 148, 259–269.
Xing, H.L., Makinouchi, A., Zhao, B.C., 2008. Three-dimensional finite element simulation of large-scale nonlinear contact friction problems in deformable rocks. J. Geophys. Eng. 5, 27–36.
Yan, P., 2013. Discussion the Genesis of Makeng Iron Ore-deposit, Fujian Province (Master Dissertation), China University of Geosciences (Beijing), Beijing (in Chinese with English Abstract).
Zhang, C., 2012. Geology and Geochemistry of Makeng Fe–Mo Deposit, Fujian (Ph. Dissertation), China University of Geosciences (Beijing), Beijing, p. 188 (in Chinese with English Abstract).
Zhang, Z., Zhang, C., 2014. Skarn mineral characteristics and zonation of the Makeng Fe–Mo deposit in Fujian Province. Acta Petrol. Sin. 30 (5), 1339–1354 (in Chinese with English Abstract).
Zhang, Z., Zuo, R., 2014. Sr–Nd–Pb isotope systematics of magnetite: implications for the genesis of Makeng Fe deposit, southern China. Ore Geol. Rev. 57, 53–60.
Zhang, Y., Hobbs, B.E., Ord, A., Barnicoat, A., 2003. The influence of faulting on host-rock permeability, fluid flow and ore genesis of gold deposits: a theoretical 2D numerical model. J. Geochem. Explor. 78-79, 279–284.
Zhang, Y., Schaubs, P.M., Barnicoat, A., 2008. Fault-related dilation, permeability enhancement, fluid flow and mineral precipitation patterns: numerical models. In: Wibberley, C.A.J., Kurz, W., Imber, J., Holdsworth, R.E., Collettini, C. (Eds.), The Internal Structure of

Fault Zones: Implications for Mechanical and Fluid-Flow PropertiesGeological Society 299. Special Publications, London, pp. 239–255.
Zhang, D., Wu, G., Di, Y., Lv, L., Yao, J., 2011. Evolution of tectonic stress field in southwestern Wuyishan Mountain area and relationship with mineralization. Geol. Bull. China 30 (4), 505–513 (in Chinese with English Abstract).
Zhang, C., Mao, J., Xie, G., Yu, M., Wang, J., Liu, W., 2012a. Geology and molybdenite Re–Os ages of Makeng Skarn-type Fe–Mo deposit in Fujian Province. J. Jilin Univ. (Earth Sci. Ed.) 42, 224–236 (in Chinese with English Abstract).
Zhang, C., Su, H., Yu, M., Hu, Z., 2012b. Zircon U–Pb age and Nd–Sr–Pb isotopic characteristics of Dayang-Juzhou granite in Longyan, Fujian Province and its geological significance. Acta Petrol. Sin. 28, 225–242 (in Chinese with English Abstract).
Zhang, C., Mao, J., Zhang, C.Q., Yu, M., 2013. Fluid inclusion characteristics and metallogenic mechanism of Makeng skarn Fe–Mo deposit in Fujian Province. Mineral Deposits 32 (2), 289–307 (in Chinese with English abstract).
Zhang, Z., Zuo, R., Cheng, Q., 2015. The mineralization age of the Makeng Fe deposit, South China: implications from U–Pb and Sm–Nd geochronology. Int. J. Earth Sci. 104, 663–682.
Zhao, C., 2009. Dynamic and Transient Infinite Elements: Theory and Geophysical, Geotechnical and Geoenvironmental Applications. Springer, Berlin.
Zhao, C., 2014. Physical and Chemical Dissolution Front Instability in Porous Media: Theoretical Analyses and Computational Simulations. Springer, Heidelberg.
Zhao, C., 2015. Advances in numerical algorithms and methods in computational geosciences with modeling characteristics of multiple physical and chemical processes. Sci. China Ser. E Technol. Sci. 58, 783–795.
Zhao, C., Hobbs, B.E., Mühlhaus, H.B., 1998. Finite element modelling of temperature gradient driven rock alteration and mineralization in porous rock masses. Comput. Methods Appl. Mech. Eng. 165, 175–187.
Zhao, C., Hobbs, B.E., Ord, A., 2008a. Investigating dynamic mechanisms of geological phenomena using methodology of computational geosciences: an example of equal-distant mineralization in a fault. Sci. China Ser. D Earth Sci. 51, 947–954.
Zhao, C., Hobbs, B.E., Ord, A., 2008b. Convective and Advective Heat Transfer in Geological Systems. Springer, Berlin.
Zhao, C., Hobbs, B.E., Ord, A., 2009. Fundamentals of Computational Geoscience: Numerical Methods and Algorithms. Springer, Berlin.
Zhao, C., Hobbs, B.E., Ord, A., 2010. Theoretical analyses of nonaqueous phase liquid dissolution-induced instability in two-dimensional fluid-saturated porous media. Int. J. Numer. Anal. Methods Geomech. 34, 1767–1796.
Zhao, C., Hobbs, B.E., Ord, A., 2012. Effects of medium and pore-fluid compressibility on chemical–dissolution front instability in fluid-saturated porous media. Int. J. Numer. Anal. Methods Geomech. 36, 1077–1100.
Zhao, C., Hobbs, B.E., Ord, A., 2013. Theoretical analyses of acidization–dissolution front instability in fluid-saturated carbonate rocks. Int. J. Numer. Anal. Methods Geomech. 37, 2084–2105.
Zhao, C., Hobbs, B.E., Alt-Epping, P., 2014. Modelling of ore-forming and geoenvironmental systems: roles of fluid flow and chemical reaction processes. J. Geochem. Explor. 144, 3–11.
Zhao, C., Hobbs, B.E., Ord, A., 2015a. Theoretical analyses of chemical dissolution-front instability in fluid-saturated porous media under non-isothermal conditions. Int. J. Numer. Anal. Methods Geomech. 39, 799–820.
Zhao, C., Hobbs, B.E., Ord, A., 2015b. Computational simulation of chemical dissolution-front instability in fluid-saturated porous media under non-isothermal conditions. Int. J. Numer. Methods Eng. 102, 135–156.
Zuo, R., Xia, Q., Zhang, D., Cheng, Q., 2012a. Geological process-based mineral resource quantitative prediction and assessment for Makeng-type iron polymetallic deposits in Fujian. Earth Sci. China Univ. Geosci. 37, 1183–1190 (in Chinese with English abstract).
Zuo, R., Cheng, Q., Carranza, E.J.M., 2012b. Fractal/multifractal modelling of geochemical exploration data. J. Geochem. Explor. 122, 1–3.
Zuo, R., Zhang, Z., Zhang, D., Carranza, E.J.M., Wang, H., 2015. Evaluation of uncertainty in mineral prospectivity mapping due to missing evidence: a case study with skarn-type Fe deposits in Southwestern Fujian Province, China. Ore Geol. Rev. 71, 502–515.